Failure characterisation in regularised media

A. Simone, H. Askes & L.J. Sluys
Faculty of Civil Engineering and Geosciences, Delft University of Technology, the Netherlands

ABSTRACT: Failure characterisation in regularised media is investigated. In this contribution it is shown that models in which the underlying continuum description is enriched through a temporal regularisation formalism (rate-dependence) perform better than models obeying spatial regularisation concept (non-locality). In particular, it is shown that a non-local dissipation-driving state variable leads to an incorrect failure characterization.

Keywords: regularised media, damage, plasticity, shear band

1 INTRODUCTION

Realistic failure characterisation, in terms of damage initiation and propagation, is a fundamental property of any sound model. A wrong prediction of the correct location or moment of initiation may lead to a misrepresentation of the failure mode and therefore of the failure load. Failure propagation is as important as failure initiation and, in a continuous failure representation, gives an indication of the failure mechanism. Aim of this contribution is to show that the choice of a non-local quantity as damage-driving quantity produces non-physical damage initiation away from the crack tip in mode I problems and a wrong failure pattern in shear band problems. In contrast, when a viscous regularisation is considered, realistic failure characterisations can be obtained.

2 REGULARISED MEDIA

Non-local and viscous regularisations were employed in this study. The reader is referred to Pijaudier-Cabot & Bažant (1987) for details on the non-local model and to Simone & Sluys (2003) for details on the viscous model. Next, a brief description of the employed regularisations is given.

In the non-local damage model considered here, damage initiation is driven by a non-local scalar measure e of the strain tensor defined as

$$e(\mathbf{x}) = \frac{\int_{\Omega} \psi(\mathbf{y};\mathbf{x}) e_l(\mathbf{y}) \, \mathrm{d}\Omega(\mathbf{y})}{\int_{\Omega} \psi(\mathbf{y};\mathbf{x}) \, \mathrm{d}\Omega(\mathbf{y})}, \tag{1}$$

where ψ is a homogeneous and isotropic weight function for the non-local averaging. The normalised Gaussian function

$$\psi(\rho) = \frac{1}{2\pi l^2} \mathrm{e}^{-\frac{\rho^2}{2l^2}} \text{ in } \mathbb{R}^2 \quad , \tag{2}$$

where l sets how ψ decays away from $\rho = 0$ and ρ is defined as the distance between the points $\mathbf{y}$ and $\mathbf{x}$, is usually taken as the weight function in integral non-local models. An approximated differential version of this non-local model (implicit gradient-enhanced damage model) has been proposed by Peerlings et al. (1996).

The viscous regularisation is provided by a rate-dependent elastoplastic-damage model which is based on the Perzyna viscoplastic model (Perzyna

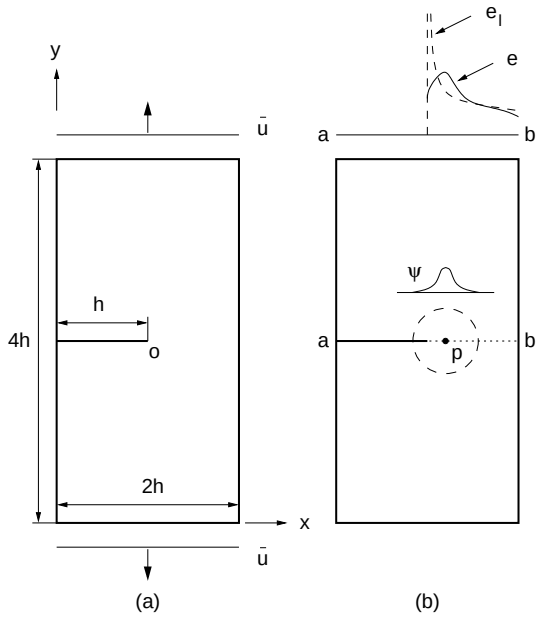

Figure 1. Compact tension specimen: (a) geometry and boundary conditions and (b) local (e) and non-local ($\bar{e}$) equivalent strain field along the crack line $\overline{ab}$.

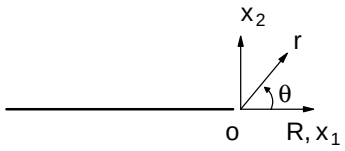

Figure 2. Linear elastic crack problem in an infinite domain.

1966) formulated in an effective stress space (Ju 1989). The basic relation reads

$$\boldsymbol{\sigma} = (1-\omega)\tilde{\boldsymbol{\sigma}}\,, \tag{3}$$

where the plastically induced damage ω ($0 \le \omega \le 1$) is updated through

$$\omega = \alpha\left(1-\mathrm{e}^{-\beta\kappa}\right) \tag{4}$$

with α and β parameters influencing the asymptotic value of damage and the slope of the damage evolution law, respectively, and κ the equivalent plastic strain in the effective space for the elastoplastic problem. In the presence of plastic flow, the viscoplastic strain rate for the Perzyna model is expressed in the associative form according to

$$\dot{\boldsymbol{\varepsilon}}^{\mathrm{vp}} = \frac{1}{\tau}\tilde{\phi}\,\tilde{\boldsymbol{f}}_{\boldsymbol{\sigma}}\,, \tag{5}$$

where τ is the relaxation time, $\tilde{\boldsymbol{f}}_{\boldsymbol{\sigma}} = \partial\tilde{f}/\partial\tilde{\boldsymbol{\sigma}}$ with $\tilde{f}$ the yield function in the effective stress space and $\tilde{\boldsymbol{\sigma}}$ the effective stress tensor, and the overstress function $\tilde{\phi}$ is given by the following power-law form

$$\tilde{\phi}\left(\tilde{f}\right) = \left(\frac{\tilde{f}}{\bar{\sigma}_0}\right)^N \tag{6}$$

with $\bar{\sigma}_0$ the initial yield stress and N ($N \ge 1$) a real number. The softening rule governing the cohesion capacity of the material is given in an exponential form according to

$$\sigma_y(\kappa) = \bar{\sigma}_0\left(\left(1+a\right)\mathrm{e}^{-b\kappa} - a\mathrm{e}^{-2b\kappa}\right), \tag{7}$$

with a and b model parameters.

3 MODE I PROBLEMS

Experimental analyses of failure initiation in quasi-brittle materials indicate that, in notched specimen, cracks initiate at the notch (van Mier 1997). Numerical investigation of crack initiation has been conducted by analysing the compact tension specimen with a pre-existing crack of length h depicted in Figure 1a. The outcome of the numerical analyses showed that the elastic contour plots of the non-local damage-driving quantity e is maximum at some distance from the crack tip, as qualitatively depicted in Figure 1b, and not at the crack tip. As a consequence, damage initiation is predicted inside the specimen, rather than at the crack tip.

Note that the crack is discretised as a set of zero measure in this example and, as such, along line $\overline{ab}$, it does not influence the integral in the denominator in (1)−the denominator in (1) is the normalising factor in the non-local averaging near free boundaries. In other words, for all points along line $\overline{ab}$ that are reasonably far from the edges of the specimen, the denominator of (1) yields the same value, therefore the shift of maximum from e_l to e is not the result of a varying averaging volume. The shift of the maximum of the non-local equivalent strain e from the crack tip is a phenomenon which is independent of the stress situation (plane stress/plane strain) and of the

choice of the local equivalent strain definition. Indeed, this phenomenon can be explained by considering that non-local averaging of the unsymmetrical local strain field e_l is performed through a symmetric function ψ . Next, an analytical consideration is presented.

For a planar crack in an infinite plate loaded in mode I, such as the one depicted in Figure 2, the linear elastic stress field is singular at the crack tip. Under the assumption of a plane stress situation, and after some analytical manipulations, the local von Mises equivalent strain

$$e_l = \frac{1}{1+\nu}\sqrt{-3J_2}\ , \tag{8}$$

where J_2 is the invariant of the strain tensor, reads (Peerlings 1999; Simone et al. 2003)

$$e_l(r,\theta) = \frac{\sqrt{2}K_1}{4E\sqrt{\pi r}}\sqrt{(1+\cos\theta)(5-3\cos\theta)}\ , \tag{9}$$

where E is the Young's modulus, ν is the Poisson's ratio and K_1 is the mode I stress intensity factor. Following Peerlings et al.(2001), it can be demonstrated that the non-local equivalent strain (1) has a finite value at the crack tip. However, this value is not the maximum, as it will be demonstrated next.

The search for larger values of the non-local equivalent strain is restricted to the points along the crack line $\overline{ab}$ (see Figure 1b). A point p is considered along line $\overline{ab}$ whereby R denotes the distance from the crack tip to p. The weight function in (2) is written for a point p as

$$\psi_p(r,\theta,R) = \frac{1}{2\pi l^2}\mathrm{e}^{-\frac{(r\cos\theta-R)^2+(r\sin\theta)^2}{2l^2}}\ , \tag{10}$$

and with this expression the non-local equivalent strain at a distance R from the crack tip along the crack line reads

$$e_R = \int_0^{\infty}\int_{-\pi}^{+\pi} \psi_p(r,\theta,R)\ e_l(r,\theta)\ r\ \mathrm{d}\theta\mathrm{d}r\ , \tag{11}$$

for which a closed form solution could not be obtained. Numerical evaluation of the integral in (11), for a given R, indicates that the maximum of the non-local equivalent strain is not positioned at the crack tip (see Figure 3). Only for $l = 0$ mm, i.e. for a local damage model, the non-local equivalent strain in (1) is maximum at the crack tip. These results extend to a finite specimen width if the effect of a finite geometry is reflected in the stress intensity factor K_I . In general, the use of non-local averaging of field quantities with isotropic weight functions results in a modification of failure characterisation. In the class of non-local elasticity models proposed by Eringen et al. (1977), the stress field value at the crack tip is finite but, similar to the non-local damage model considered here, its maximum occurs at some distance from the crack tip along the crack line.

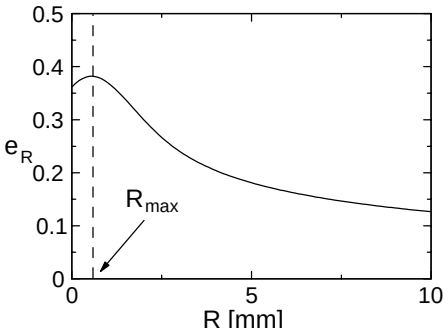

Figure 3. Non-local equivalent strain at distance R from the tip for $l = 1$ mm and unit values of E and K_1 .

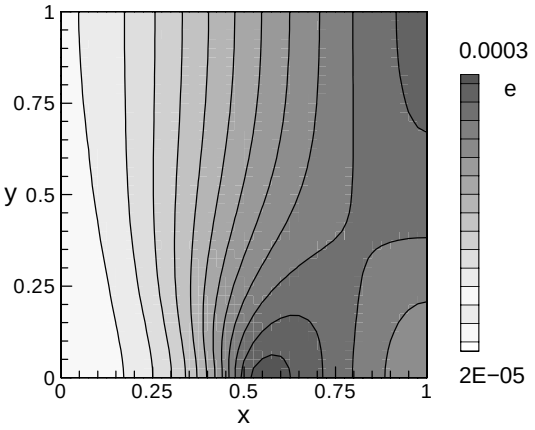

Figure 4. Contour plot of the non-local equivalent strain for the differential non-local damage model at the onset of damage initiation, i.e. in the elastic stage (measures in mm; crack tip at $x = 0.5$ mm).

The compact tension specimen depicted in Figure 1a has been numerically analysed by using a differential non-local damage model with the finite-element method. In the numerical simulations only the upper part of the specimen has been discretised due to symmetry, and the load has

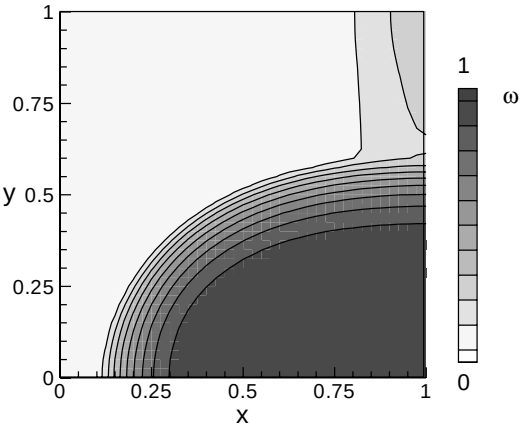

Figure 5. Contour plot of the damage field for the differential non-local damage model close to failure (measures in mm; crack tip at $x = 0.5$ mm).

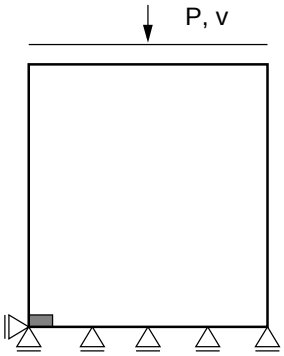

Figure 6. Geometry and boundary conditions for the specimen in biaxial compression; the shaded part indicates the imperfection (specimen size is $h \times h$; imperfection size is $h/10 \times h/20$; $h = 60$ mm).

been applied via an imposed displacement. The following have been adopted for the simulation: Young's modulus E=1000 MPa; Poisson's ratio $\nu = 0$; exponential damage evolution law

$$\omega = 1 - \frac{\kappa_0}{\kappa}\left(1 - \alpha + \alpha \mathrm{e}^{-\beta(\kappa - \kappa_0)}\right) \text{ if } \kappa > \kappa_0 , \qquad (12)$$

where κ is a history parameter related to the non-local equivalent strain, with the threshold of damage initiation $\kappa_0 = 0.0003$ and softening parameters $\alpha = 0.99$ and $\beta = 1000$, length scale $l = 0.2$ mm and the equivalent strain definition according to Mazars (1984):

$$e_l = \sqrt{\sum_{i=1}^{3} \langle \varepsilon_i \rangle^2} , \qquad (13)$$

with $\langle \varepsilon_i \rangle = \left(\varepsilon_i + |\varepsilon_i|\right)/2$ and ε_i the principal strains. The height of the specimen has been taken as $4h$ = 2 mm. The mesh used for the simulations has been chosen such that a sufficient resolution of the non-local field is obtained. More details on the finite-element implementation of the differential non-local model can be found in Peerlings et al. (1996). The non-local equivalent strain at the onset of damage initiation is reported in Figure 4. Clearly, the maximum of the non-local equivalent strain has shifted. Due to the shifting, damage is expected to initiate, wrongly, away from the crack tip. However, as depicted in Figure 5, the damage contour plot close to global failure of the specimen gives no indication of the incorrect damage initiation. Experience with the differential version of the non-local damage model indicates that this is a common situation in mode I problems and that failure characterisation close to failure is quite similar to the ones obtained with other constitutive models. Consequently, the shift of the maximum of the non-local equivalent strain away from the crack tip can be considered `harmless' as long as the final failure characterisation is concerned. However, it must be realised that the use of a non-local dissipation-driving variable leads to a non-physical damage initiation. The shift of the maximum of the non-local equivalent strain away from the crack tip is present, although less evident, also in case of cracks or notches modelled as strongly non-convex entities with non-zero volume, i.e. when there are no strain singularities. Similar analyses were performed with a rate-dependent elastoplastic-damage model and damage initiation was correctly predicted at the crack tip.

4 SHEAR BAND PROBLEMS

The correct determination of shear bands is of prime interest and it is directly linked to the occurrence of possible collapse mechanisms in many engineering problems. Specimens under compressive loading are usually characterised by the formation of shear bands whose inclination can be determined analytically. Results obtained within the flow theory of plasticity (Runesson et al. 1991) have been extended to scalar damage models by Rizzi et al. (1995) and Carol & Willam (1997) and apply to an infinite geometry for a standard (i.e. not regularised) medium. Their results have been derived for a specific choice of the equivalent strain definition and their generalisation to other equivalent strain definitions, although possible in

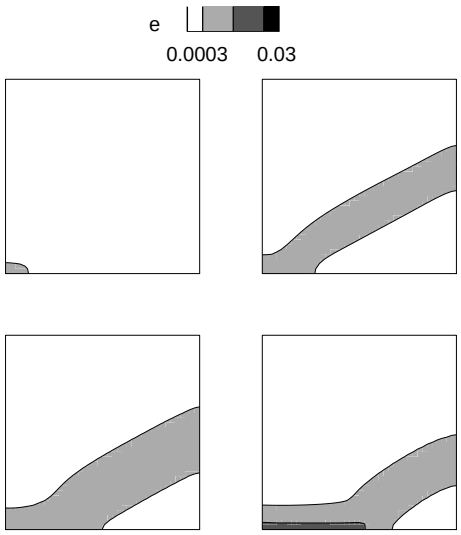

Figure 7. Shear band evolution: contour plots of the non-local equivalent strain field.

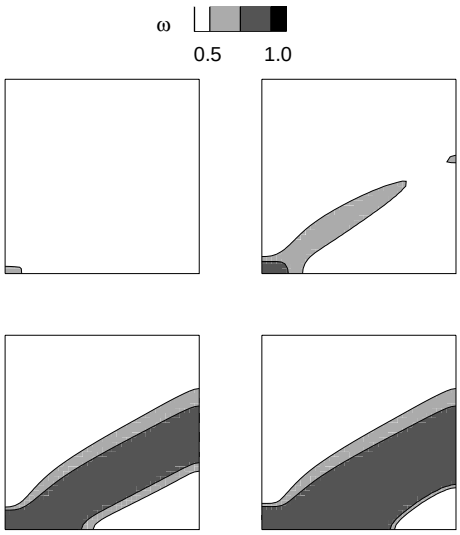

Figure 8. Shear band evolution: contour plots of the damage evolution.

principle, is not within the scope of this study and is therefore not considered here. In what follows, it is illustrated how non-local regularisation techniques significantly alter failure propagation during strain localisation.

To illustrate the problem, shear band simulations under a plane stress and a plane strain configuration have been performed with the gradient-enhanced continuum damage model proposed by Peerlings et al. (1996) for the two-dimensional specimen depicted in Figure 6. In numerical simulations of quasi-static shear band formation under compressive loading, shear bands are usually triggered by an imperfection (positioned at the left bottom corner of the specimen in Figure 6). After the shear band has been initiated, expansion of the plastic zone and further localisation within the plastic zone is observed (Zervos et al. 2001). Shear bands are characterised by their stationary nature in the sense that their position is more or less fixed after their formation (see Nemat-Nasser & Okada (2001) and references herein for experimental shear bands and Tvergaard et al. (1981), Ortiz et al. (1987), Sluys (1992), Garaizar & Trangenstein (1998), Zervos et al. (2001), Borja (2000) and Wells at al. (2002) for numerical results). The inclination angle that the shear band forms with the horizontal axis is determined mainly by assumptions related to the constitutive model, to the Poisson's ratio and to the plane stress or plane strain condition (Runesson et al. 1991; Sluys 1992; Rizzi et al. 1995; Carol & Willam 1997) while the width of the shear band is dictated by the length scale (i.e. the larger the length scale, the wider the band width).

In the numerical analyses, the material has been given the Young's modulus E = 20000 MPa, the Poisson's ratio ν = 0.2, the exponential softening law (12) with $\kappa_0 = 0.0001$, $\alpha = 0.99$ and $\beta = 300$ and the von Mises equivalent strain (8). The load has been applied via displacement control. The imperfection has been given a reduced value of κ_0 ($\kappa_0 = 0.00005$) and the mesh density has been chosen to ensure a sufficient resolution of the non-local field. To begin with, the evolution of the shear band, in terms of non-local equivalent strain and damage fields has been analysed for the specimen in Figure 6 with a length scale $l = 2$ mm under a plane strain condition. Results are depicted in Figures 7 and 8. In the contour plots in Figures 7 and 8, only values larger than the threshold in the respective legends have been plotted. It is clear that the shear band "migrates" from the weak spot, where it was initiated, to the opposite side of the specimen along the horizontal boundary. Similar results are reported by Engelen et al. (2003) and Pamin et al. (2003). This failure mode is due to a wrong prediction of the positioning of localised shearing and has the same nature of the shift of the maximum of the non-local equivalent strain in mode I problems. The effect of a larger length scale is reported in Figure 9 together with a comparison between plane stress and plane strain conditions

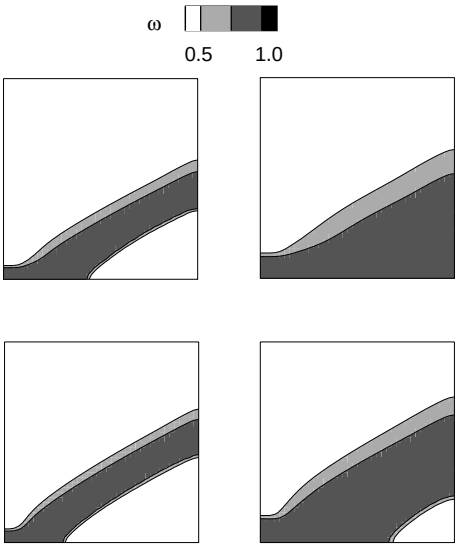

Figure 9. Shear band close to failure: contour plots of the damage field for $l = 1$ mm (left) and $l = 2$ mm (right) for plane stress (top) and plane strain (bottom).

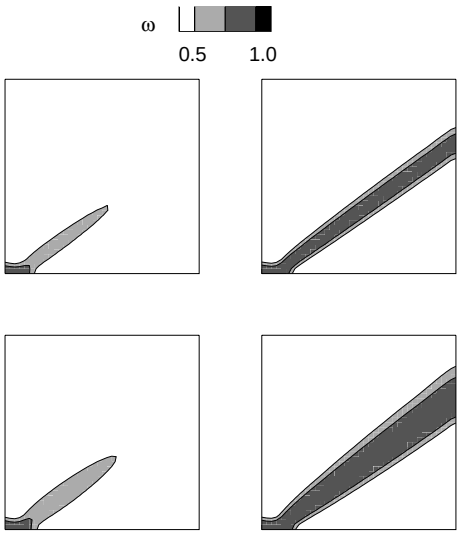

Figure 10. Shear band evolution: contour plots of the damage field with the rate-dependent elastoplastic-damage model for $\tau = 4$ s (top) and $\tau = 8$ s (bottom) at the beginning of the localisation process (left) and close to failure (right).

close to failure. Similar to shear bands in a plasticity context (Runesson et al. 1991) and as reported by Carol & Willam (1997), the only noticeable difference between plane stress and plane strain resides in a different inclination of the shear band with respect to the horizontal axis which does not correspond to the numerical results in Figure 9 where the shear band has moved from the left hand side to the right end side with the shift being more pronounced in the plane stress situation. Further, with an increasing non-local effect a wider shear band width is expected, while it is also noted that a more pronounced shift (to the right hand side of the specimen) of the shear band takes place.

The shear band problem was also analysed with a rate-dependent elastoplastic-damage model. The simulations were performed with a von Mises plane stress rate-dependent damage-elastoplasticity model for two values of the relaxation time τ in (5). Other model parameters are: Young's modulus $E = 20000$ MPa, Poisson's ratio $\nu = 0.2$, $N = 1$ in (6), softening parameters $a = -1$ and $b = 200$ in (7) and $\alpha = 0.99$ $\beta = 300$ in (4) and yield stress equal to 2 MPa with a reduction of 10% in the weak region. The total displacement was applied at constant displacement rate (for $\tau = 4$ s the final displacement (0.08 mm) was applied in 160 equal steps with $\Delta v = 0.0005$ mm while for $\tau = 8$ s the final displacement (0.2 mm) was applied in 400 equal steps with $\Delta v = 0.0005$ mm). Results are reported in Figure 10. The shear band evolves correctly, is stationary and its width is set by the relaxation time. The slight shift of the shear band is due to the rectangular geometry of the imperfection and is not influenced by the relaxation time (see Section 3).

5 CONCLUDING REMARKS

When non-local averaging is considered as a regularisation technique, the use of a non-local variable as degradation-driving variable induces incorrect failure initiation in mode I problems and incorrect failure propagation in shear band problems. Although the shift of the maximum of the dissipation-driving variable may not alter the final failure representation in mode I dominated problems, it does affect the transition from continuous to continuous-discontinuous failure in a gradient-enhanced damage model as discussed in Simone et al. (2003). The numerical study of a shear band problem illustrated that the non-local averaging is responsible for a non-stationary–like shear band which results in an unrealistic failure pattern. This has been studied for various length scale values under plane stress and plane strain conditions. The shear band problem was also analysed with a rate-dependent elastoplastic-damage model which gave correct results. To

summarise, constitutive models based on a non-local dissipation-driving variable may lead to incorrect failure initiation and propagation in arbitrary loading scenarios due to a fundamental flaw in damage characterisation. Their use is acceptable with some reserve only in mode I problems. These findings are not limited to damage mechanics but extend easily to other dissipation mechanisms, e.g. plasticity (Engelen et al. 2003; Pamin et al. 2003), if a similar form of regularisation is employed.

ACKNOWLEDGEMENTS

Financial support to AS through the BEO programme (special fund from TU Delft for excellent research) is gratefully acknowledged.

REFERENCES

Borja, R. I. 2000. A finite element model for strain localization analysis of strongly discontinuous fields based on standard Galerkin approximation. *Computer Methods in Applied Mechanics and Engineering 190*, 1529−1549.

Carol, I. & Willam, K. 1997. Application of analytical solutions in elasto-plasticity to localization analysis of damage models. In D. R. J. Owen, E. Onate, & E. Hinton (Eds.), *Computational Plasticity, Fundamentals and Applications*, Barcelona, Spain, pp. 714−719. CIMNE.

Engelen, R. A. B., Geers, M. G. D. & Baaijens, F. P. T. 2003. Nonlocal implicit gradient-enhanced elasto-plasticity for the modelling of softening behaviour. *International Journal of Plasticity 19*(4), 403−433.

Eringen, A. C., Speziale, C. G. & Kim, B. S. 1977. Crack-tip problem in non-local elasticity. *Journal of the Mechanics and Physics of Solids 25,* 339−255.

Garaizar, F. X. & Trangenstein, J. 1998. Adaptive mesh refinement and front-tracking for shear bands in an antiplane shear model. *SIAM Journal on Scientific Computing 20*(2), 750−779.

Ju, J. W. 1989. On energy-based coupled elastoplastic damage theories: constitutive modeling and computational aspects. *International Journal of Solids and Structures 25*(7), 803−833.

Mazars, J. 1984. *Application de la Mécanique de l'Endommagement au Comportement Non-Linéaire et à la Rupture du Béton de Structure*. Ph. D. thesis, Université Paris VI, France.

van Mier, J. G. M. 1997. *Fracture Processes of Concrete.* Boca Raton, Florida: CRC Press, Inc.

Nemat-Nasser, S. & Okada, N. 2001. Radiographic and microscopic observation of shear bands in granular materials. *Géotechnique 51*(9), 753−765.

Ortiz, M., Leroy, Y. & Needleman, A. 1987. A finite element method for localized failure analysis. *Computer Methods in Applied Mechanics and Engineering 61*, 189−214.

Pamin, J., Askes, H. & de Borst, R. 2003. Two gradient plasticity theories discretized with the Element-free Galerkin Method. *Computer Methods in Applied Mechanics and Engineering 192*, 2377−2403.

Peerlings, R. H. J. 1999. *Enhanced Damage Modelling for Fracture and Fatigue.* Ph. D. thesis, Eindhoven University of Technology.

Peerlings, R. H. J., de Borst, R., Brekelmans, W. A. M. & de Vree, J. H. P. 1996. Gradient-enhanced damage for quasi-brittle materials. *International Journal for Numerical Methods in Engineering 39*, 3391−3403.

Peerlings, R. H. J., Geers, M. G. D., de Borst, R. & Brekelmans, W. A. M. 2001. A critical comparison of nonlocal and gradient-enhanced softening continua. *International Journal of Solids and Structures 38*, 7723−7746.

Perzyna, P. 1966. Fundamental problems in viscoplasticity. In *Advances in Applied Mechanics*, Volume 9, pp. 243−377. New York: Academic Press.

Pijaudier-Cabot, G. & Bažant, Z. P. 1987. Nonlocal damage theory. *Journal of Engineering Mechanics 113*, 1512−1533.

Rizzi, E., Carol, I. & Willam, K. 1995. Localization analysis of elastic degradation with application to scalar damage. *Journal of Engineering Mechanics 121*(4), 541−554.

Runesson, K., Ottosen N. S. & Peric, D. 1991. Discontinuous bifurcation of elasto-plastic solutions in plane stress and plane strain. International Journal of Plasticity *7*, 99−121.

Simone, A., Wells, G. N. & Sluys, L. J. 2003. From continuous to discontinuous failure in a gradient-enhanced continuum damage model. *Computer Methods in Applied Mechanics and Engineering 192*(41−42), 4581−4607.

Simone, A., Askes, H. & Sluys, L. J. 2004. Incorrect initiation and propagation of failure in non-local and gradient-enhanced media. *International Journal of Solids and Structures.* In press.

Simone, A. & Sluys, L. J. 2004. The use of displacement discontinuities in a rate-dependent medium. *Computer Methods in Applied Mechanics and Engineering*. In press.

Sluys, L. J. 1992. *Wave Propagation, Localisation and Dispersion in Softening Solids*. Ph. D. thesis, Delft University of Technology.

Tvergaard, V., Needleman, A. & Lo, K. K. 1981. Flow localization in the plane strain tensile test. *Journal of the Mechanics and Physics of Solids 29* (2), 115−142.

Wells, G. N., Sluys, L. J. & de Borst, R. 2002. Simulating the propagation of displacement discontinuities in a regularised strain-softening medium. *International Journal for Numerical Methods in Engineering 53*(5), 1235−1256.

Zervos, A., Papanastasiou, P. & Vardoulakis, I. 2001. A finite element displacement formulation for gradient elastoplasticity. *International Journal for Numerical Methods in Engineering 50*, 1369−1388.